Analysis of an *x*-cut Ti:$LiNbO_3$ Electrooptic Modulator with a Ridge Structure by the Finite Element Method

Nancy M. Abe, Marcos A. R. Franco, Angelo Passaro, and Francisco Sircilli

Instituto de Estudos Avançados – Centro Técnico Aeroespacial – São José dos Campos – SP

***Abstract* — An analysis of a Mach-Zehnder Ti:$LiNbO_3$ traveling-wave electrooptic modulator with a ridge structure is presented in this work. The performance of the device is studied assuming *x*-cut substrate. Two configurations employing ridge structure are compared to a conventional one. This work also presents the influence of some fabrication parameters of the optical waveguide on the factors which evaluates the efficiency of the modulators. The characteristics of both the optical waveguide and the coplanar waveguide electrode are computed applying the scalar finite element method.**

***Index terms* — integrated optics, optical waveguides, coplanar waveguides, ridge waveguides, electrooptic modulation, finite element method**.

I. Introduction

Electrooptic modulators have widespread use in optical communication systems, optical signal processing, and optical computing. In recent years, several modulators structures have been investigated to achieve large modulation bandwidth with a low driving voltage. The coplanar waveguide shape, the introduction of buffer layers, the reduction of the substrate thickness, and shielding planes are some of the characteristics that can be introduced and optimized in order to improve the modulators performance [1]-[8].

This work presents an analysis of a Ti:$LiNbO_3$ traveling-wave electrooptic modulator employing a ridge structure. The study focuses on the lossless device behavior assuming an *x*-cut substrate. Two ridge structure configurations are compared to a conventional one. An analysis of the influence of some optical waveguide fabrication parameters, such as the diffusion temperature and the width of the titanium strip, on the efficiency of the modulators is also presented.

The Finite Element Method (FEM) was applied to analyze the microwave and the optical propagation properties. The microwave electric field was computed by applying the quasi-TEM approximation and the optical propagation properties were computed from the scalar wave equation.

II. The Finite Element Formulations

A. Quasi-Static Analysis – TEM Modes

The quasi-TEM modes are related to the solutions of the Laplace equation for the electric potential ϕ:

$$\nabla \cdot \left(\bar{\varepsilon}_r \ \nabla \phi \right) = 0 , \tag{1}$$

where the relative permittivity tensor is given by:

$$\bar{\varepsilon}_r = \begin{bmatrix} \varepsilon_{xx} & 0 \\ 0 & \varepsilon_{yy} \end{bmatrix} \tag{2}$$

The finite element method applied to (1) yields the matrix equation

$$[S]\{\phi\}^T = \{b\}^T , \tag{3}$$

where:

$$[S] = \int_{\Omega} \left(\varepsilon_{xx} \ \{N\}_x^T \ \{N\}_x + \varepsilon_{yy} \{N\}_y^T \ \{N\}_y \right) dx dy , \tag{4}$$

$$\phi = \{N\}\{\phi\}^T ,$$

$$\vec{E} = - \nabla \phi ,$$

$\{\ \}$ represents a row matrix, $\{\ \}^T$ stands for a transposed matrix and $\{N\}$ represents a complete set of base functions for the used finite elements. $\{N\}_x$ and $\{N\}_y$ represent the partial derivative of the base functions in x and y, respectively.

B. Optical Modes

The modal analysis of the Ti:$LiNbO_3$ waveguide was carried out by a scalar finite element implementation for both nonhomogeneous and anisotropic media [9], [10].

The Helmholtz equation in the scalar approximation, for a lossless, nonhomogeneous and anisotropic dielectric optical waveguide with diagonal relative permittivity tensor, and a harmonic *z*-propagating wave, can be expressed for the E^x modes as

$$\begin{aligned} & n_z^2 \frac{\partial}{\partial x}\left(\frac{1}{n_z^2} \right) \frac{\partial \left(n_x^2 E_x \right)}{\partial x} + \frac{\partial^2 \left(n_x^2 E_x \right)}{\partial x^2} \\ & + n_z^2 \frac{\partial^2 E_x}{\partial y^2} + k_0^2 \, n_x^2 \, n_z^2 \, E_x = n_z^2 \beta^2 E_x , \end{aligned} \tag{5}$$

and for the E^y modes as follows

$$\begin{aligned} & \frac{\partial^2 H_x}{\partial x^2} + n_y^2 \frac{\partial}{\partial y}\left(\frac{1}{n_z^2} \frac{\partial H_x}{\partial y} \right) \\ & + n_y^2 k_0^2 H_x = \beta^2 H_x \end{aligned} \tag{6}$$

where k_0 is the free space wavenumber and β is the propagation constant. The variables $n_x(x,y)$ and $n_y(x,y)$ are the refractive indexes in the transversal x and y directions

respectively, and $n_z(x,y)$ is the refractive index in the longitudinal direction.

The application of the Weighted Residual Method with the Galerkin Approximation in (5) and (6) yields the matrix equation

$$[F]\{\phi\}^T = n_{eff}^2 [M]\{\phi\}^T , \tag{7}$$

where $n_{eff} = \beta / k_0$ is the effective index [9]-[11]. The matrices for each finite element are given by:

$$[M] = \int_{\Omega} \boldsymbol{A}\ k_0^2\ \{N\}^T \{N\}\, dx\, dy , \tag{8}$$

$$[F] = [F_1] - [F_2]. \tag{9}$$

The parameter $\boldsymbol{A}$ and the matrices $[F_1]$ and $[F_2]$ depend on the propagation modes.

For the E^x modes $\boldsymbol{A} = n_z^2$ and the matrices are:

$$[F_1] = \int_{\Omega} \left(k_0^2\, n_x^2\, n_z^2\, \{N\}^T \{N\} - n_x^2\, \{N\}_x^T \{N\}_x\right) dx\, dy - \int_{\Omega} n_z^2\, \{N\}_y^T \{N\}_y\ dx\, dy \tag{10}$$

and

$$[F_2] = \int_{\Omega} \left(\delta_x \frac{\partial n_x^2}{\partial x} \{N\}_x^T \{N\} + \delta_z \frac{\partial n_z^2}{\partial y} \{N\}^T \{N\}_y \right) dx\, dy - \int_{\Omega} \delta_z \{N\}^T n_z^2\ \frac{\partial g_z^2}{\partial x} \left(\delta_x \frac{\partial n_x^2}{\partial x} \{N\} + n_x^2\ \{N\}_x \right) dx\, dy \tag{11}$$

For E^y modes $\boldsymbol{A} = 1$,

$$[F_1] = \int_{\Omega} \left[k_0^2\, n_y^2\ \{N\}^T \{N\} - \{N\}_x^T \{N\}_x \right] dx\, dy - \int_{\Omega} n_y^2\, g_z^2\, \{N\}_y^T \{N\}_y\ dx\, dy \tag{12}$$

and

$$[F_2] = -\int_{\Omega} \delta_y\ g_z^2\ \frac{\partial n_y^2}{\partial y}\ \{N\}^T\ \{N\}_y\, dx\, dy - \int_{\Omega} \delta_z\ n_y^2 \left(\frac{\partial g_z^2}{\partial y} + g_z^4 \frac{\partial n_z^2}{\partial y} \right) \{N\}^T\ \{N\}_y\, dx\, dy\ , \tag{13}$$

For both propagation modes $g_z = 1/n_z$. The parameters δ_x and δ_z assume either the value 1 for diffused index in the x and z directions respectively, or zero for constant index. The matrix $[F_2]$ is sparse and nonsymmetrical because of the presence of terms with partial derivative of the refractive index.

In this work, the variation of the refractive indexes and their spatial derivatives inside each finite element are expanded in terms of the first order Lagrange type base functions $\{N\}$:

$$n_i^2 = \{N\}\left\{n_i^2\right\}^T , \quad i, j = x, y, z$$

$$\frac{\partial n_i^2}{\partial j} = \{N\}_j \left\{n_i^2\right\}, \qquad \frac{\partial g_z^2}{\partial j} = \{N\}_j \left\{g_z^2\right\}$$

III. Ti:$LiNbO_3$ Channel Optical Waveguide

The effect of the following manufacturing parameters are considered to define the optical channel waveguide: the initial width of the Ti strip, W, the initial thickness of the Ti strip, H, the ion diffusion temperature, T, and the ion diffusion time, t. Additionally, the parameters were chosen to guarantee the complete diffusion of Ti into the $LiNbO_3$ substrate avoiding the presence of residual titanium oxide films which cause scattering losses and increase insertion loss.

For Ti:$LiNbO_3$ channel waveguides, the refractive index in the diffused region follows [14]:

$$n_{e,o}^2(x,y,\lambda) = n_{b_{e,o}}^2 + \left[\left(n_{b_{e,o}} + \Delta n_{s_{e,o}} \right)^2 - n_{b_{e,o}}^2 \right] exp\left(-\frac{y^2}{d_y^2} \right) f\left(\frac{2x}{W} \right), \tag{14}$$

where:

$$f\left(\frac{2x}{W}\right) = \frac{1}{2}\left\{ erf\left[\frac{W}{2d_x}\left(1 + \frac{2x}{W}\right)\right] + erf\left[\frac{W}{2d_x}\left(1 - \frac{2x}{W}\right)\right]\right\},$$

e and o denote the extraordinary and ordinary principal crystal axes respectively, x and y are the coordinates of a point in the substrate, d_x and d_y are the diffusion width and depth respectively, n_b is the substrate refractive index and Δn_s stands for the variation of the surface index with the wavelength.

In addition, $\Delta n_{se,o}$ is given in terms of H and some additional fitting parameters [12] :

$$\Delta n_{s_{e,o}}(\lambda) = \left[B_0(\lambda) + B_1(\lambda) \frac{H}{d_{y_{e,o}}} \right] \left(\frac{H}{d_{y_{e,o}}} \right)^{\alpha_{e,o}} , \tag{15}$$

$$\alpha_e = 0.83, \quad \alpha_o = 0.53, \quad 0.6 \le \lambda(\mu m) \le 1.6$$

$$B_{0e}(\lambda) = 0.385 - 0.430\lambda + 0.171\lambda^2 ,$$

$$B_{1e}(\lambda) = 9.130 + 3.850\lambda - 2.490\lambda^2 ,$$

$$B_{0o}(\lambda) = 0.0653 - 0.0315\lambda + 0.0071\lambda^2 ,$$

$$B_{1o}(\lambda) = 0.4780 + 0.4640\lambda - 0.3480\lambda^2 .$$

The diffusion coefficients D_x and D_y, the diffusion width d_x and depth d_y and the depth of refractive index change profiles d_{ye} and d_{yo} can be calculated by the Arrhenius Law:

$$D_i = D_{i0}\, exp\left(-E_{i0}/kT\right), \quad i = x, y \tag{16}$$

$$d_i = 2\sqrt{D_i\, t}\ , \quad i = x, y \tag{17}$$

$$d_{y_{e,o}} = \frac{d_y}{\sqrt{\alpha_{e,o}}}, \quad (18)$$

where D_{i0} is the diffusion constant, E_{i0} is the activation energy and k is the Boltzmann constant. The constants for Ti-diffused $LiNbO_3$ are presented in Table I [12].

Table 1.Coefficients of the Arrhenius Law for Ti:$LiNbO_3$ Guides.

D_{x0} (μm^2 / h)	5.0 e+9
D_{y0}(μm^2 / h)	1.35 e+8
E_{x0} (eV)	2.60
E_{y0} (eV)	2.22

The refractive indexes dispersion of the SiO_2 and of the $LiNbO_3$ are taken into account by using the three-terms Sellmeier equation for SiO_2 and the equivalent relations for $LiNbO_3$ presented in [11].

IV. ANALYSIS

The cross-sectional view of the analyzed structure is shown in Fig.1 The magnified region shows geometrical details of the ridge. The buffer layer thickness d on the horizontal plane is larger than the thickness b along the side wall. This difference results from the fabrication process. The design and fabrication techniques of an optical modulator with this kind of structure are described in [4], for a z-cut $LiNbO_3$ substrate.

The numerical analysis was performed for a wavelength of 1.523 μm considering the geometry shown in Fig.1. The inclination α of the ridge side walls is assumed equal to 70º, compatible with the values obtained in experimental measurements [4]. The ridge height h and the electrode gap g are assumed to be 3.5 μm and 15 μm, respectively. The guide is built in a x-cut $LiNbO_3$ substrate.

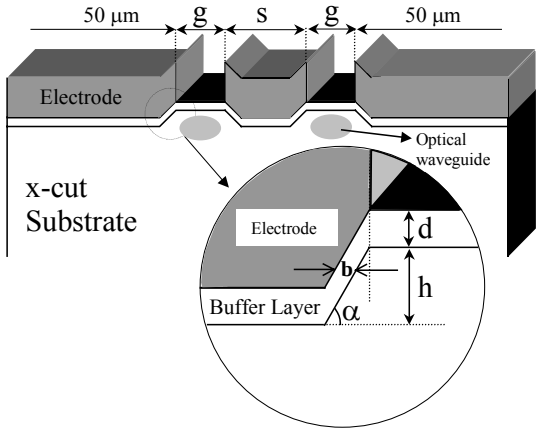

Fig. 1. The cross-sectional view of the Ti:$LiNbO_3$ Mach-Zehnder traveling-wave electrooptic modulator employing a ridge structure and a detail of the ridge.

The half-wave voltage, the driving power, the characteristic impedance, the microwave effective index, the overlap integral and the modulation bandwidth are used to evaluate the optical modulators performance. The microwave effective index and the characteristic impedance are given by [3]:

$$N_{eff} = \sqrt{\frac{C}{C_o}} \quad (19)$$

$$Z_c = \frac{1}{c\sqrt{C_o C}} \quad (20)$$

where c is the velocity of light in vacuum, C and C_0 are the capacitance per unit length of the CPW when the dielectric material is considered and when it is replaced by vacuum, respectively.

The modulation-frequency bandwidth Δf for the lossless traveling-wave modulators is given by [13]:

$$\Delta f = \frac{1.4\ c}{\pi \left| N_{eff} - n_{eff} \right| L} \quad (21)$$

where L is the interaction length, n_{eff} and N_{eff} are the effective index for the optical and the quasi-TEM modes, respectively.

The overlap integral factor Γ, for each optical waveguide, the half-wave voltage V_π and the driving power modulation P_{in}, are calculated as follows [3], [6]:

$$\Gamma = \frac{g}{V} \frac{\iint E_{op}^2(x,y)\, E_{TEM}(x,y)\, dxdy}{E_{op}^2(x,y)\, dxdy} \quad (22)$$

$$V_\pi = \frac{\lambda_o\, g}{n_e^3\, r_{33} \left(\left|\Gamma_1\right| + \left|\Gamma_2\right| \right) L} \quad (23)$$

$$P_{in} = \frac{V_\pi^2}{8 Z_s \left[1 - \left(\frac{Z_s - Z_c}{Z_s + Z_c} \right)^2 \right]} \quad (24)$$

where g is the gap between the electrodes (Fig. 1), V is the applied voltage, E_{op} is the optical electric field, E_{TEM} is the component of the microwave electric field, λ_o is the free space optical wavelength, n_e is the extraordinary refractive index of the substrate, r_{33} is the electrooptic coefficient of $LiNbO_3$, Γ_1 and Γ_2 are the overlap integral factors for each one of the optical guides of the modulator and Z_s is the impedance of the microwave source. For x-cut Ti:$LiNbO_3$ waveguides symmetrically positioned in relation of the central electrode, $|\Gamma| = |\Gamma_1| = |\Gamma_2|$.

A. Variation of the Electrode Thickness

Three configurations were considered to perform this analysis. Two of them employ ridge structures, as shown in Fig.1, and the other one has conventional characteristics - i.e. it presents rectangular shaped electrodes and the interface between the buffer layer and the substrate is a plane that is represented by a straight line for a 2D analysis. The width of the central electrode and the thickness of the buffer layer for these configurations are shown in Table I.

The fabrication conditions of the optical waveguide for the results presented in this section are 3 hours of

diffusion time at 1050 °C and initial Ti strip width and thickness of 5 μm and 80 nm, respectively [9], [14].

Table 2. Electrode width and buffer layer thickness

Configuration		Central electrode width s (μm)	Buffer layer thickness d (μm)
A	Ridge	5	2.5
B	Ridge	8	1.5
C	Conventional	8	1.5

For the studied configurations, both the electrical effective index N_{eff} and the characteristic impedance Z_c are shown in Fig. 2 as a function of the electrode thickness.

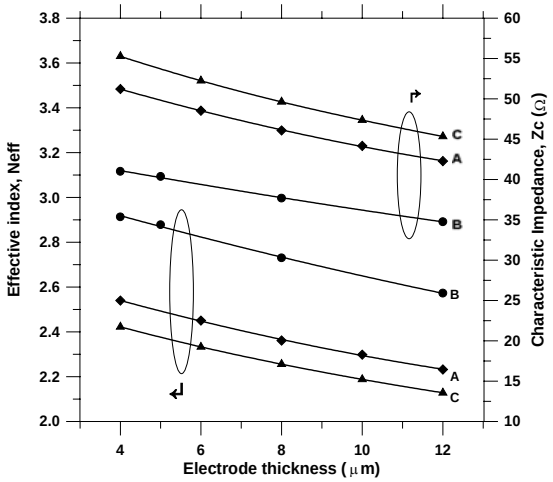

Fig. 2. Effective index N_{eff} and characteristic impedance Z_c as a function of the electrode thickness, for the configurations A, B and C of Table 2.

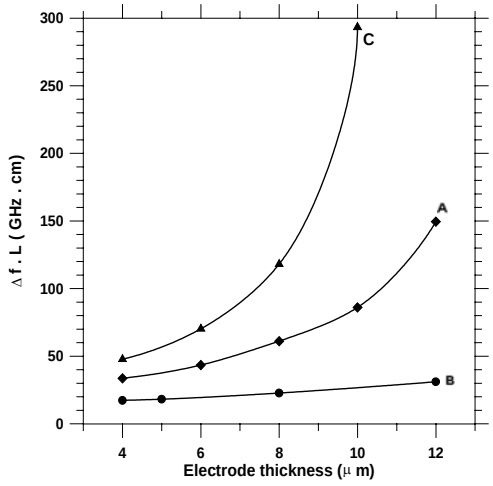

Fig. 3. $\Delta f L$ product as a function of the electrode thickness, for the configurations A, B and C.

The behavior of the product $\Delta f L$ is shown in Fig. 3 while Fig. 4 shows the variation of the products $V_\pi L$ and $P_{in} L^2$. In this analysis, it was assumed impedance Z_s of 50 Ω and the microwave losses were not considered. The configurations A and C provide better characteristics for impedance and velocity matching conditions while configurations A and B (ridge structure) present lower values of the product $V_\pi L$.

The configuration B presents the lowest modulation bandwidth but it presents the smallest driving power values for a given electrode length. Additionally, as the influence of the electrode thickness on parameters Δf, V_π and P_{in} is small, the control on the electrodes deposition process would not need to be too rigorous for this configuration.

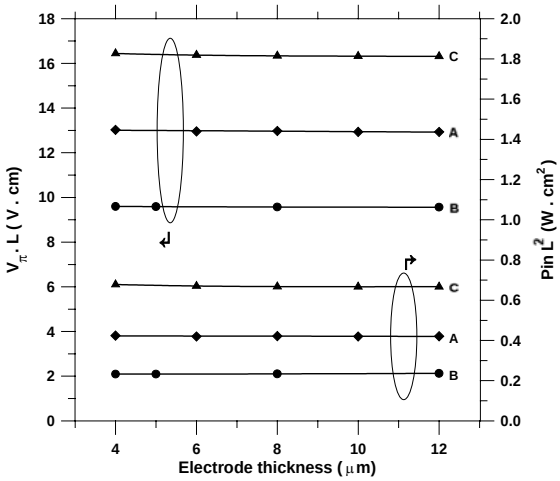

Fig. 4. $V_\pi L$ product and $P_{in} L^2$ product as a function of the electrode thickness, for the configurations A, B and C.

B. Variation of the Buffer Layer Thickness

The results presented in this section correspond to the configurations A and B, assuming the electrodes thickness of 8 μm and 4 μm, respectively. The same optical waveguide fabrication parameters described in section *A* were used. The electrical effective index N_{eff} and the characteristic impedance Z_c are shown in Fig. 5 as a function of the buffer layer thickness. The product $\Delta f L$ is shown in Fig. 6 and the overlap integral factor is presented in Fig. 7. The products $V_\pi L$ and $P_{in} L^2$ are shown in Fig. 8.

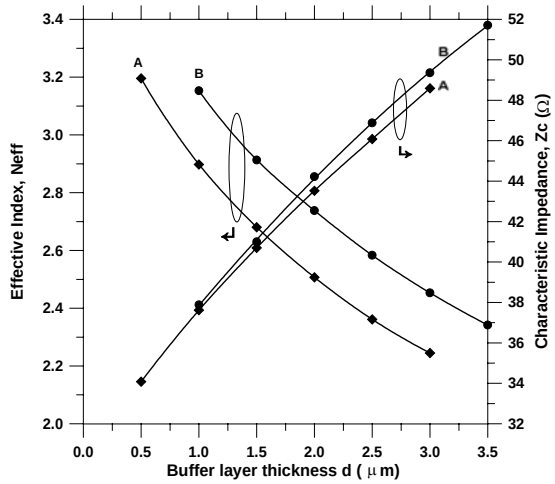

Fig. 5. Effective index N_{eff} and characteristic impedance Z_c as a function of the buffer layer thickness, for both configurations A and B.

The driving power for the configuration B (Fig. 8) reaches approximately the same value of the one obtained for the conventional configuration (Fig. 4), when the buffer layer thickness d equals to the ridge height h = 3.5 μm. We should remember, however, that the buffer layer thickness of the configuration C for the results presented in Fig. 4 is 1.5 μm.

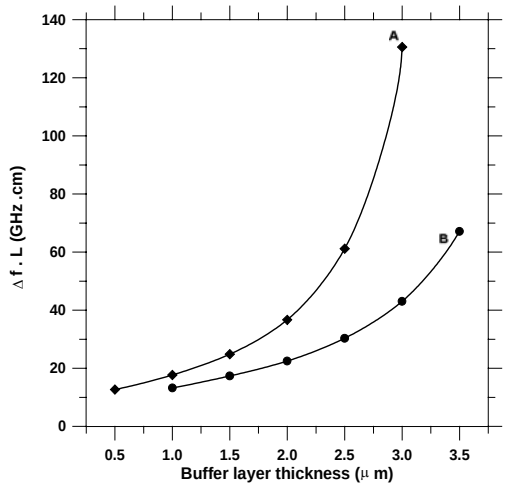

Fig. 6. Δf L product of the modulation-frequency bandwidth and the interaction length as a function of buffer layer thickness, for both configurations A and B.

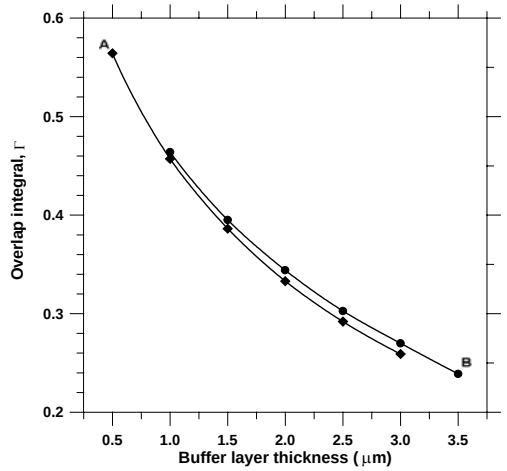

Fig. 7. Overlap integral factor as a function of the buffer layer thickness, for both configurations A and B.

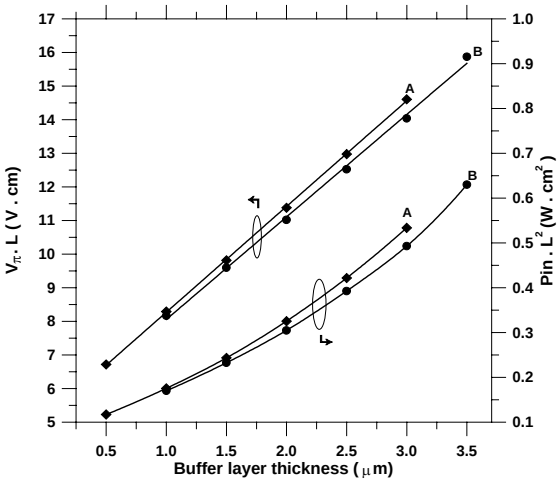

Fig. 8. $V_\pi L$ and $P_{in} L^2$ products as functions of the buffer layer thickness, for both A and B configurations.

C. Variation of the Optical Waveguide Fabrication Conditions

In this section, the behavior of the modulator is presented as a function of some of the optical waveguide fabrication conditions, namely, the diffusion temperature, the diffusion time and the initial Ti strip width. For this purpose, the configuration A with an electrode thickness of 8 μm has been adopted.

The optical mode profiles in the diffused region were calculated following the method presented in [9], [10], [14]. This method is suitable for computing the optical mode profiles for the ridge structure waveguide since the Ti diffusion is carried out before the etching procedure. Otherwise, the geometry of the substrate could affect the Ti diffusion.

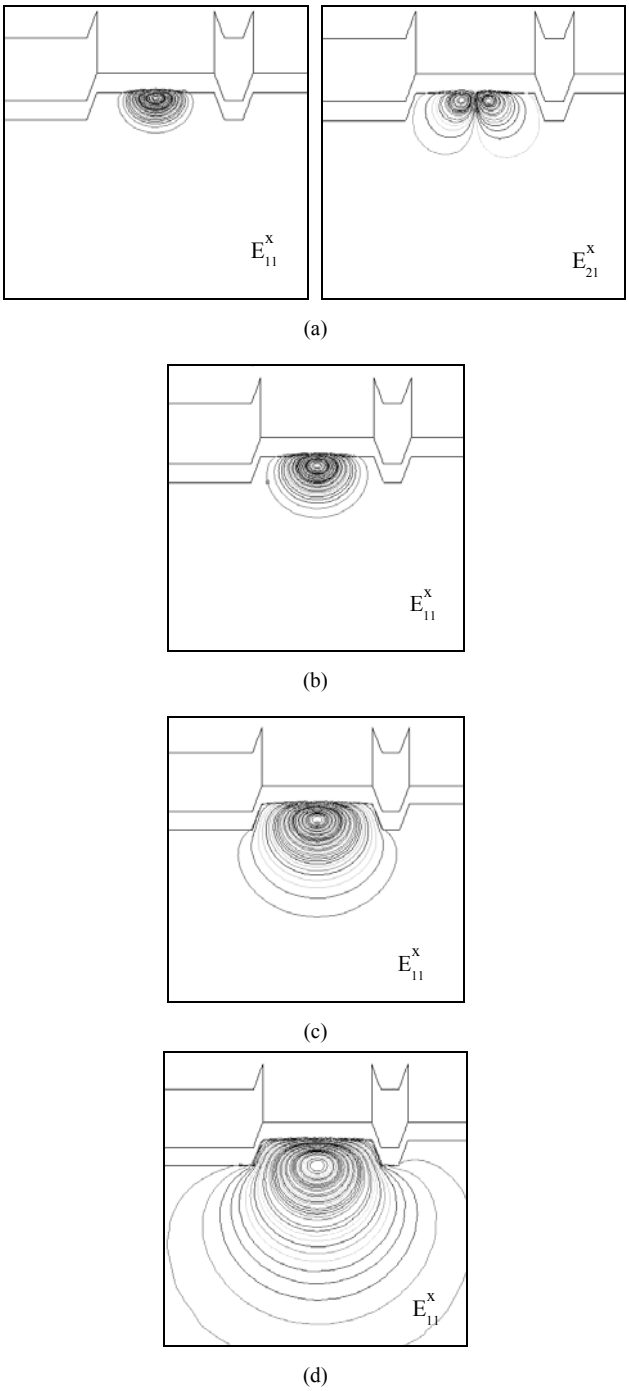

Fig. 9. Evolution of the optical mode profile as a function of the diffusion temperature (a) 1000 °C, (b) 1050 °C, (c) 1100 °C and (d) 1150 °C.

A symmetric Gaussian function and a Hermite-Gaussian trial solution are often used to approximately represent the fundamental mode profile in weakly guiding

optical waveguides . However, to use these functions the optical mode sizes should be known. As the mode sizes depend on the fabrication parameters, they need to be determined *a priori* either by empirical means or by some other technique. Moreover, these approximations should not provide accurate optical field profiles for waveguides built in complex geometric structures. The application of numerical analysis, like the one adopted in this work, allows obtaining careful descriptions of the mode profiles.

Fig. 9 shows the evolution of the optical modes profile (optical spots) as a function of the diffusion temperature, assuming 5 μm and 80 nm of initial Ti strip width and thickness, respectively, and 3 h of diffusion time. Under these fabrication conditions, the obtained results showed that the monomode operation for E^x modes is reached for temperatures higher than 1000 °C, Fig. 10.

The products $V_\pi L$ and $P_{in} L^2$ as a function of the diffusion temperature are shown in Fig. 11. As the diffusion temperature increases, the fundamental optical mode spreads out through the substrate. This leads to a decrease of the overlap integral and both the $V_\pi L$ and $P_{in} L^2$ products increase.

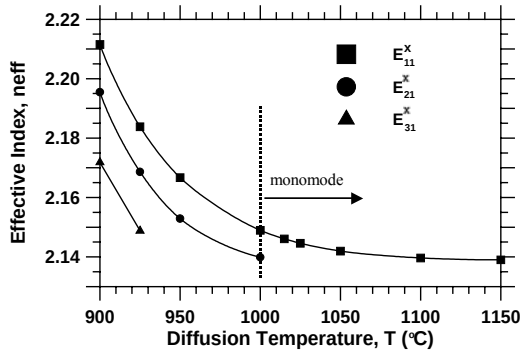

Fig. 10. Effective index for the three first optical modes as a function of the Ti-layer diffusion-process temperature.

Notice that mode profiles resembling that presented in Fig. 9(d), can occur for temperatures lower than 1150 °C. Other fabrication conditions or different geometric parameters, such as a small electrode gap, can lead to a similar behavior.

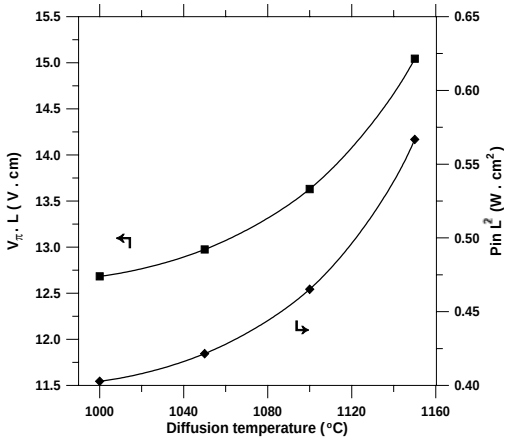

Fig. 11. $V_\pi L$ product and $P_{in} L^2$ product as a function of the diffusion temperature.

$V_\pi L$ and $P_{in} L^2$ products are shown in Fig. 12 as a function of the diffusion time for a initial Ti strip width and thickness of 5 μm and 80 nm, respectively. If the diffusion is carried out for a long time, the working characteristics of the modulator become worse, although the waveguide keeps on monomode condition.

Fig. 13 shows the products $V_\pi L$ and $P_{in} L^2$ as a function of the initial Ti strip width for a diffusion time of 3 h at 1050 °C and 80 nm of Ti strip thickness. The half-wave voltage and the driving modulation power decrease slightly as the initial Ti strip width increases. However, the monomode operation is achieved for Ti strip widths smaller than 7 μm (Fig. 14).

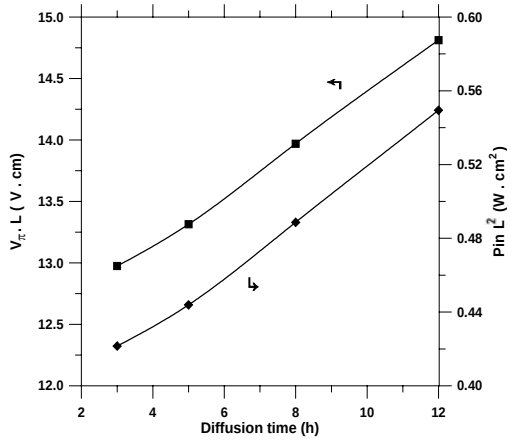

Fig. 12 - $V_\pi L$ product and $P_{in} L^2$ product as a function of the diffusion time.

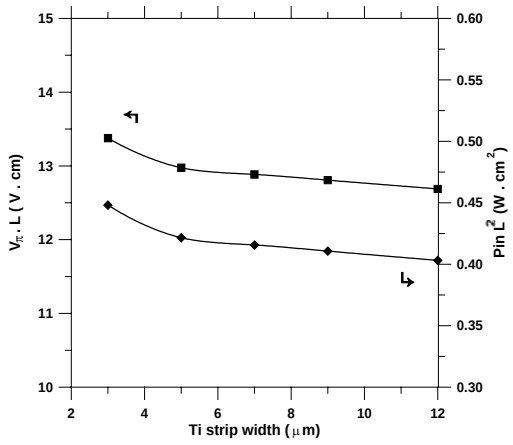

Fig. 13. $V_\pi L$ product and $P_{in} L^2$ product as a function of the initial Ti strip width.

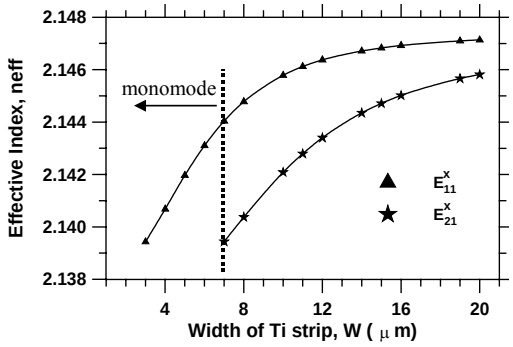

Fig. 14. Effective index as a function of the initial width of Ti strip.

V. CONCLUSION

A scalar FEM formulation was applied to compute both the traveling-wave electrical characteristics and the optical waveguide propagation properties of a x-cut Ti:$LiNbO_3$ electrooptic modulator with a ridge structure. Two configurations employing ridge structure were compared to a conventional one. The study also included a numerical analysis of the electrooptic modulator behavior as a function of the fabrication parameters of the optical waveguide.

The analyzed modulators employing ridge structure can provide lower power consumption than the conventional one does. However, the velocity mismatch debases their wide-band applications. Even so, profitable operation conditions were established for this kind of modulators. One of the studied configurations reduces substantially the microwave driving power with a $V_\pi L$ product lower than 10 V.cm at a $\Delta f L \cong 20$ GHz.cm condition. The other one can be used in applications that require larger modulation bandwidth ($\Delta f L \cong 60$ GHz.cm for an electrode thickness of 8 μm) but with a $V_\pi L$ product of 13 V.cm.

ACKNOWLEDGEMENTS

The authors wish to thank FAPESP for partial financial support of this work (proc. 98/07789-7).

REFERENCES

[1] H. Jin, M. Bèlanger and Z. Jakubczyk, "General Analysis of Electrodes in Integrated-Optics Electrooptic Devices", *IEEE Journal of Quantum Electronics*, vol. 27, No. 2, pp. 243-251, Feb. 1991.

[2] K. Kawano, "High-Speed Shielded Velocity-Matched Ti:$LiNbO_3$ Optical Modulator", *IEEE Journal of Quantum Electronics*, vol. 29, No. 9, pp. 2466-2475, Sept. 1993.

[3] X. Zhang and T. Miyoshi, "Optimum Design of Coplanar Waveguide for $LiNbO_3$ Optical Modulator", *IEEE Transactions on Microwave Theory and Techniques*, vol. 43, No. 3, pp. 523-528, March 1995.

[4] K. Noguchi, O. Mitomi, H. Miyazawa and S. Seki, "A Broadband Ti:$LiNbO_3$ Optical Modulator with a Ridge Structure", *Journal of Lightwave Technology*, vol. 13, No.6 , pp. 1164-1168, June 1995.

[5] N. H. Zhu, E. Y. B. Pun and P. S. Chung, "Analysis of Shielded Coplanar Waveguide with Trapezoidal Electrodes", *IEEE Photonics Technology Letters*, vol. 8, No. 2, pp. 242-244, Feb. 1996.

[6] K. W. Hui, K. S. Chiang, B. Wu and Z. H. Zhang, "Electrode Optimization for High-Speed Traveling-Wave Integrated Optic Modulators", *Journal of Lightwave Technology*, vol. 16, No. 2, pp. 232-238, Feb. 1998.

[7] M. Koshiba, Y. Tsuji and M. Nishio, "Finite Element Modeling of Broad-Band Travelling-Wave Optical Modulators," *IEEE Transactions on Microwave Theory and Techniques*, vol.47, No.9, pp. 1627-1633, Sept. 1999.

I.-L. Gheroma, P. Savi, and R.M. Osgood, Jr., "Thin Layer Design of X-Cut $LiNbO_3$ Modulators," *IEEE Photonics Technology Letters*, vol. 12, No. 12, pp. 1618-1620, Dec. 2000.

[9] M. A. R. Franco, A. Passaro, J. R. Cardoso, and J. M. Machado, "Finite Element Analysis of Anisotropic Optical Waveguide with Arbitrary Index Profile", *IEEE Transactions on Magnetics*, vol.35, No.3, pp.1546-1549, May 1999.

[10] M. A. R. Franco, A. Passaro, F. Sircilli Neto, J. R. Cardoso, and J. M. Machado, "Modal Analysis of Anisotropic Diffused-Channel Waveguide by a Scalar Finite Element Method", *IEEE Transactions on Magnetics*, vol. 34, No. 5, pp.2783-2786, Sept. 1998.

[11] M. Koshiba, *Optical Waveguide Theory by the Finite Element Method*, 1st ed., KTK Scientific Publishers/Kluwer Academic Publishers, Tokyo/Dordrecht, The Netherlands, 1992.

[12] S. Fouchet, A. Carenco, C. Daguet, R. Guglielmi, and L. Riviere, "Wavelength Dispersion of Ti Induced Refractive Index Change in $LiNbO_3$ as a Function of Diffusion Parameters," *J. Lightwave Technol.*, vol. LT-5, N. 5, pp. 700-708, May 1987.

[13] H. Nishihara, M. Haruna, and T. Suhara, *Optical Integrated Circuits,* 1st ed., McGraw-Hill, 1989, pp.109-111.

[14] D. Zhang, C. Chen, J. Li, G. Ding, X. Chen, and Y. Cui, "A Theoretical Study of a Ti-Diffused Er:$LiNbO_3$ Waveguide Laser," *IEEE Journal of Quantum Electronics*, vol. 32, No. 10, pp. 1833-1838, Oct. 1996.

Nancy Mieko Abe obtained the B.Sc. and M.Sc. degrees in electrical engineering from the Escola Politécnica da Universidade de São Paulo (EPUSP), Brazil, in 1989 and 1992, respectively. In 1997, she obtained the doctorate degree in electrical engineering from the same university (EPUSP). In 1998, she joined the Institute for Advanced Studies of Aerospace Technical Center (IEAv-CTA), Brazil, as a researcher fellow. Since 2002 she is an Adjunct Researcher in the Virtual Engineering Laboratory of IEAv/CTA. Her research interests include electromagnetic field computation, heat conduction analysis, plasma simulation, numerical methods and high-performance parallel programming.
(email: nancy@ieav.cta.br)

Marcos Antonio Ruggieri Franco was graduated in Physics at Pontifícia Universidade Católica de São Paulo – Brazil (PUC-SP), in 1983. In 1991, he finished his Master of Science degree in Nuclear Physics at Intituto de Física da Universidade de São Paulo-Braxil (IFUSP). In 1999, he received his doctorate in Electrical Engineering from the Escola Politécnica da Universidade de São Paulo – Brazil (POLI-USP). In 1987, he joined the research team of the division of Applied Physics at Institute for Advanced Studies (IEAv) at Dentro Técnico Aeroespacial (CTA). Since 2001, he is also associated professor of the pos-graduate course of Electronic Computation Engineering from the Instituto Tecnológico de Aeronáutica (ITA). His major areas of interest are the application of the Finite Element Method for the design of electromagnetic devices sucha as microwave and optical waveguides, fiber optics, integrated optics, antennas and electromagnetic scattering problems.
(email: marcos@ieav.cta.br)

Angelo Passaro received the B.Sc. in physics (1981) and the M.Sc degrees in nuclear physics (1988) from the Instituto de Física da Universidade de São Paulo (IFUSP), Brazil. In 1998, he completed his doctorate degree in electrical engineering at the Escola Politécnica da Universidade de São Paulo (EPUSP), Brazil. In 1984, he joined the Institute for Advanced Studies of Aerospace Technical Center. Since 1999, he has been the head of the Virtual Engineering Laboratory of (IEAv-CTA). His current research interests are in high-performance parallel programming, numerical methods, electromagnetic field computation, plasma simulation, and heat conduction analysis.
(email:angelo@ieav.cta.br)

Francisco Sircilli Neto was graduated at the Institute of Physics of São Paulo University (IFUSP), Brazil, in 1981. His Master Science was obtained in 1986 at the National Institute for Space Research (INPE), Brazil, in the area of Nuclear Geophysics. In 1997 he concluded his Doctorate in Electrical Engineering at the Polytechnic School of São Paulo University (POLI-USP), Brazil. Since 1985 he joined the research team of Division of Applied Physics of the Institute for Advanced Studies of the Aerospace Technical Center (IEAv/CTA). Today his main area of interest is the application of the Finite Element Method (FEM) to wave propagation in devices such as microwave, optical waveguides and fiber optics, as well as to antennas and electromagnetic scattering problems.
(email: sircilli@ieav.cta.br)